Lattice dynamics and related diffusion properties of intermetallics: I. Fe_3Si

1995 J. Phys.: Condens. Matter 7 5983

(http://iopscience.iop.org/0953-8984/7/30/005)

J. Phys.: Condens. Matter 7 (1995) 5983–5999. Printed in the UK

Lattice dynamics and related diffusion properties of intermetallics: I. Fe_3Si

O G Randl†‡, G Vogl‡, W Petry§, B Hennion‖, B Sepiol‡ and K Nembach¶

† Institut Laue–Langevin, BP 156X, 38042 Grenoble Cédex 9, France

‡ Institut für Festkörperphysik der Universität Wien, 1090 Wien, Austria

§ Physikdepartment E13, TU München, 85748 Garching, Germany

‖ Laboratoire Léon Brillouin, CEN Saclay, 91191 Gif-sur-Yvette, France

¶ Institut für Metallforschung, WWU Münster, 48149 Münster, Germany

Received 27 February 1995, in final form 10 April 1995

Abstract. The phonon dispersion of iron-rich Fe–Si alloys of $D0_3$ structure (space group $Fm-3m$) has been studied by inelastic neutron scattering. The measurements were carried out on two crystals of different composition: $Fe_{75}Si_{25}$ at 20 and 930 °C, and $Fe_{80}Si_{20}$ at 20, 930 and 1100 °C. The respective degree of order was determined by powder diffraction measurements. A general decrease of phonon frequencies with increasing temperature is found, the temperature dependence being strongest for transverse phonons with [ξξ0] propagation. With decreasing order, phonon gaps close and the highest optical band degenerates into a broad distribution of inelastic intensity due to disorder scattering. The dependence of the dispersion on the alloy composition is not very pronounced. The migration enthalpies as well as several other thermodynamic quantities have been calculated from the densities of states. Although the low frequencies of the transverse phonons indicate particularly low migration barriers, they cannot explain the pronounced change of the diffusivity with composition. This composition dependence is tentatively explained by high vacancy concentrations.

1. Introduction

Many intermetallic alloys show very high self-diffusivities, sometimes as high as or even higher than those measured in monatomic BCC metals like β-Ti or β-Zr. In general, the diffusion coefficients strongly depend on the alloy composition. The diffusion mechanism in some of these alloys has been investigated directly by quasielastic neutron scattering (NiSb by Vogl *et al* (1993), and Ni_3Sb by Sepiol *et al* (1994)) and Mössbauer spectroscopy (Fe_3Si and FeAl by Sepiol and Vogl (1993) and Vogl and Sepiol (1994) and Feldwisch *et al* (1995)). For instance, it has been found that the iron atoms of stoichiometric Fe_3Si of $D0_3$ structure (space group $Fm-3m$) perform only nearest-neighbour jumps between the two different iron sublattices. However, at even slightly off-stoichiometric concentrations, jumps via antistructure sites on the silicon sublattice contribute strongly. One possible reason for the high diffusivities might be found in the similarity of the $D0_3$ structure to the monatomic BCC structure. In fact, Petry *et al* (1989) have been able to establish a link between fast diffusion and anomalies in the phonon dispersion of BCC metals ('phonon-enhanced diffusion'). Thus, the question arises if (i) anomalously fast diffusion in intermetallics and (ii) its dependence on alloy composition can be related to phonon anomalies.

The primitive unit cell of the $D0_3$ structure is shown in figure 1(*a*). In a perfectly ordered alloy of stoichiometric composition, there is one sublattice populated exclusively by Si atoms (usually referred to as β)—the remaining three sites per primitive unit cell are

0953-8984/95/305983+17$19.50

occupied by Fe atoms. For reasons of symmetry, two of the three Fe sites are equivalent, so we distinguish two Fe sublattices: α (four Fe and four Si nearest neighbours) and γ (all the nearest neighbours are Fe atoms).

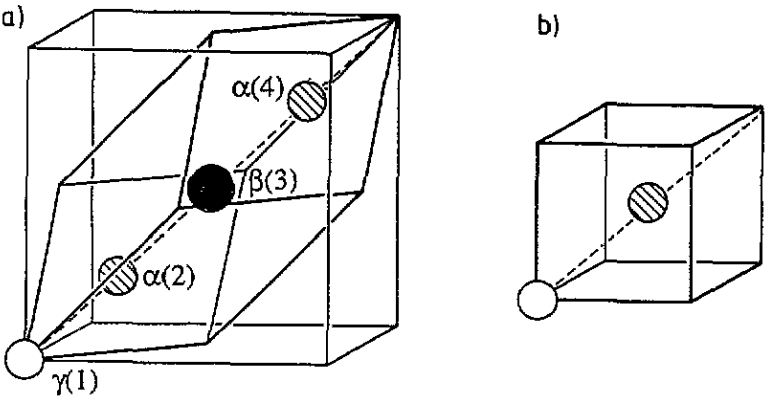

Figure 1. The primitive unit cells of the structures of the alloys examined in this paper. (*a*) The $D0_3$ structure. There are four atoms on three symmetrically different sites in the primitive unit cell. In the case of perfect order, the α and γ sites are occupied by Fe, the β sites by Si atoms. The indexation of these sites ($i = 1, \ldots, 4$) is noted in brackets. (*b*) The B2 or CsCl structure. In B2-ordered phases of Fe–Si alloys that are formed from $D0_3$ structures upon disordering, one of the two sites is occupied by an Fe atom, the other by a statistical mixture of Fe and Si atoms.

When the alloy composition is changed or the temperature is raised, disorder is introduced. The nature of the disordering mechanism is controversial. According to Kubaschewski (1982) *Fe–Si alloys in the range from 10 to 20 at.% show a second-order* phase transition to the B2 (CsCl) phase at high temperatures. In the B2 structure, Si occupies both the β and γ sublattices; the primitive unit cell of this structure is shown in figure 1(*b*). At even higher temperatures, the alloy disorders completely. Then Si is statistically distributed over all sublattices and the BCC structure is adopted. Recently, Hilfrich *et al* (1993, 1994) have found indications for $D0_3$ long-range order in Fe–Si alloys of up to 20 at.% Si, even in regions where the phase diagram of Kubaschewski (1982) predicts B2 order. They conclude that the disordering at high temperatures consists of the creation of antistructure boundaries between small $D0_3$-ordered domains. It is not within the scope of the present investigation to decide between these two competing models, but some conclusions can be drawn, as will be shown later on.

There is only little published experimental information on phonon dispersions of systems with $D0_3$ order. The most intensely studied system is Fe_3Al. After a first meticulous study of its room-temperature dispersion by Van Dijk (1970a, b), the different states of order of quenched alloys have been examined by Robertson (1985, 1991), and at present high-temperature investigations are being undertaken by Kentzinger *et al* (1995). Zolliker (1992) has studied the phonon dispersion of Cu–Zn–Al in detail. Some selected phonon branches of Cu–Al–Ni (Morii and Iizumi 1985) and Au–Cu–Zn (Mori *et al* 1975) have been measured near the martensitic phase transition. Finally, there are some phonon data on Fe_3Si in the literature: Pintschovius (1987) has measured magnetic excitations in Fe_3Si at 660 °C and determined four phonon branches in order to separate the nuclear from the magnetic intensities.

2. Samples and experimental details

The three single crystals used in this study were grown by the Bridgman method (sample A, $Fe_{75}Si_{25}$) and by zone melting (sample B, $Fe_{75}Si_{25}$, and sample C, $Fe_{80}Si_{20}$). All the crystals showed a mosaic spread of about 1°.

The iron content of sample A was checked by wet chemical analysis as well as by analysing the room-temperature Mössbauer spectra (the method is described in Rixecker *et al* (1993)) and found to be 75.5 ± 0.3 at.%. Sample C was examined by microprobe analysis and found to have an iron concentration of 80.3 ± 0.4 at.%.

All three samples were cylindrical (A, $l = 11$ mm, $r = 5$ mm; B, $l = 53$ mm, $r = 2$ mm; C, $l = 32$ mm, $r = 2$ mm) and of $\langle 011 \rangle$ orientation, i.e. the $\langle 011 \rangle$ direction was parallel to the cylinder axis. In this plane almost all the phonons in the main symmetry directions can be measured; but in order to measure the transverse $T_1[\xi\xi 0]$ (polarization $[\xi\ -\xi 0]$) branch, the crystals were tilted in the $\langle 001 \rangle$ direction by means of a specially constructed Nb sample holder. The fine adjustment of the crystal in the measuring plane was done by means of two goniometers on which the furnace was tilted.

During the measurements, the order of the single crystals was checked by measuring the intensity of superlattice lines on the three-axis spectrometer. Although this method does not allow one to determine the degree of order to as high a precision as diffraction measurements, it allowed us to see which phase was present. In particular, it became clear that the ordering dynamics of the iron-rich Fe–Si alloys is quite fast, which is in agreement with earlier findings (e.g. Dokken 1965). The equilibrium states were reached almost instantaneously at high temperatures. It is difficult to decide if the same is true for the samples measured at room temperature, but the state we reached by natural cooling from 1100°C to room temperature (which took about 3 h) was at least metastable, since it did not change even after several weeks.

Inelastic neutron scattering measurements were performed on the three-axis spectrometer 1-T of the Orphée reactor of the Laboratoire Léon Brillouin (LLB). Most of the scans were performed with constant final wavevector $k_f = 2.66$ Å^{-1}, using a PG(002) monochromator and analyser as well as a graphite filter to suppress $\lambda/2$ contributions. Some high-energy optical phonons were measured using a copper(111) monochromator. No additional horizontal collimations were used; the effective horizontal collimation was 25′/30′/50′/50′.

All the measurements were performed with the sample mounted in an ILL standard resistance furnace (Ibel 1994). The vacua obtained were of the order of 10^{-6} mbar or better, even at high temperatures. The sample temperature was measured with two independent thermocouples. The nominal temperature was stable to ±2 °C, and the absolute error at high temperatures is estimated to be of the order of 10 °C.

The measurements have been carried out at several different temperatures: at 20 and 930 °C for $Fe_{75}Si_{25}$ and at 20, 930 and 1100 °C for $Fe_{80}Si_{20}$.

3. Conventions

Some conventions have to be followed in order to describe the phonon branches and the underlying force constants unambiguously. The direction of propagation of a phonon branch is referred to by a capital Greek letter ($\Delta \simeq [\xi 00]$, $\Sigma \simeq [\xi\xi 0]$, $\Lambda \simeq [\xi\xi\xi]$), and the irreducible representation to which the branch belongs by a subscript number. In the $D0_3$ structure we find the following irreducible representations: Δ_1, Δ_3, Δ_5, Σ_1, Σ_2, Σ_3, Σ_4, Λ_1, Λ_3; in the B2 structure: Δ_1, Δ_3, Σ_1, Σ_3, Σ_4, Λ_1, Λ_3. Finally, the branches of a given

irreducible representation are numbered by a superscript integer in brackets, in ascending order from the low-energy acoustic modes to the highest optical modes. We have also measured some off-symmetry phonons in the B2 structure ($[\xi, \frac{1}{2}\frac{1}{2}]$ direction), which are denoted by $\Pi^{(1)}$ and $\Pi^{(2)}$.

Unfortunately, there is no unique convention in the literature for the force constants. In harmonic approximation the equation of motion for atom i in the elementary cell l of a crystal reads:

$$m_i \frac{d^2 u_{il}}{dt^2} = -\sum_{i',l'} \tilde{V}_{il,i'l'} u_{i'l'}$$

where m_i is the mass of atom i (i running from 1 to N_c, the number of atoms in the elementary cell), u_{il} is the displacement of atom i in cell l from its equilibrium position, and $\tilde{V}_{il,i'l'}$ is the matrix of second derivatives of the pair potential between the atoms at (il) and $(i'l')$.

We use a Born–von Kármán (BVK) model in the axial approximation, i.e. we assume the matrix $\tilde{V}_{il,i'l'}$ to be of the form

$$\tilde{V}_{il,i'l'} = [T_n(ii') - L_n(ii')] \begin{bmatrix} r_x^2 & r_x r_y & r_x r_z \\ r_x r_y & r_y^2 & r_y r_z \\ r_x r_z & r_y r_z & r_z^2 \end{bmatrix} - T_n(ii') \begin{bmatrix} 1 & 0 & 0 \\ 0 & 1 & 0 \\ 0 & 0 & 1 \end{bmatrix}$$

where

$$(r_x, r_y, r_z) = (r_{i'l'} - r_{il})/|r_{i'l'} - r_{il}|$$

and r_{il} is the equilibrium position of atom i in cell l. The $L_n(ii')$ are called longitudinal and the $T_n(ii')$ transverse force constants of the n-nearest-neighbour interaction between atoms of type i and atoms of type i'.

4. Results

4.1. Phonon dispersion

The phonon frequencies we have measured (in both constant-energy and constant-q mode) are available from the authors upon request. The data are shown in figures 2–4, together with the BVK model fits (which will be discussed in the next section).

As the measuring time was limited, not all the phonon branches could be studied. Measurements in the region of 10 THz were complicated by the fact that there are spurious inelastic scattering intensity peaks of the PG monochromator in this energy range. Intensity peaks at these energies were interpreted as phonons only if they could be followed in reciprocal space. Some selected phonons of high symmetry were checked by using a copper monochromator, but this leads to a great loss in intensity and unreasonably long measuring times. In any case, the phonons observed at highest energies have to be interpreted cautiously.

Three effects are clearly visible from figures 2–4. First, the phonon frequencies of both alloys depend on temperature: the lattice becomes distinctly softer as the temperature is increased. The zone-boundary $\Sigma_3^{(1)}$ phonon (T[$\xi\xi$0] with polarization [ξ $-$ ξ0]), for example, drops from about 4 THz at room temperature to values around 3 THz at 930 °C,

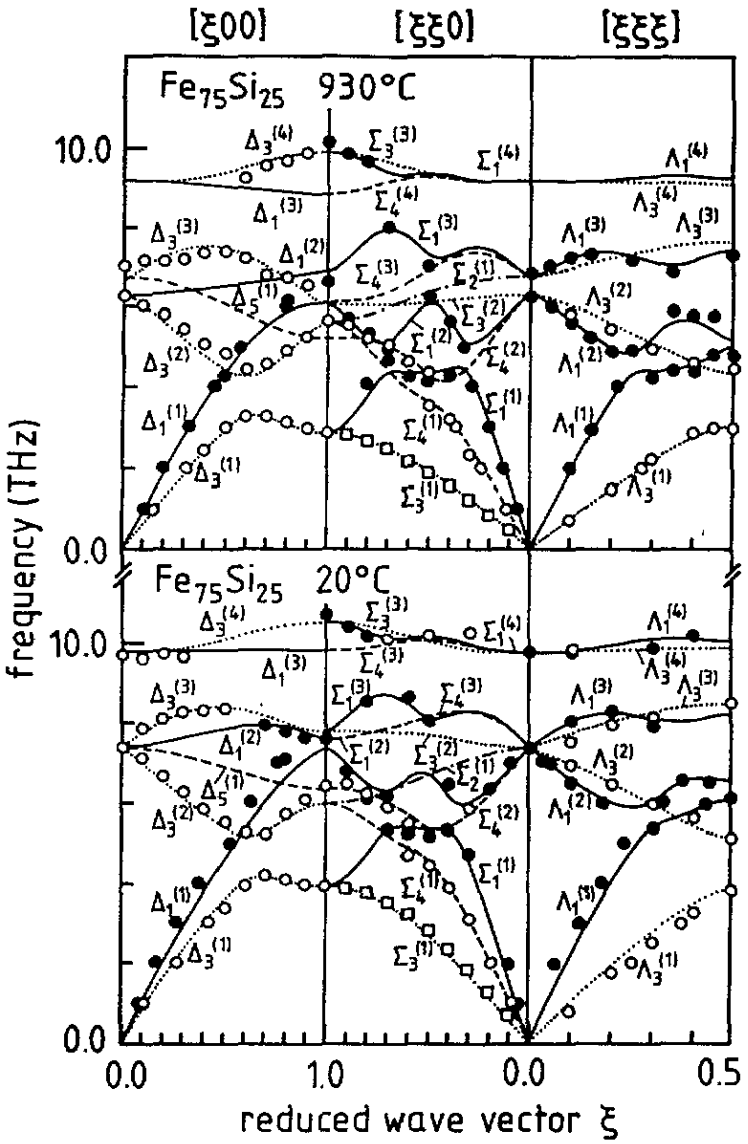

Figure 2. $Fe_{75}Si_{25}$: phonon dispersion at 20 and 930 °C. The lines correspond to a BVK fit assuming $D0_3$ structure and interactions between up to fourth nearest neighbours.

in both $Fe_{75}Si_{25}$ and $Fe_{80}Si_{20}$, and decreases further to 2.6 THz at 1100 °C for $Fe_{80}Si_{20}$. This softening is rather general and not restricted to particular branches or regions in reciprocal space, but the branches of lower energy are more strongly concerned than the high-energy ones.

Secondly, the dispersions of the two alloys are very similar at the same temperature. However, phonon gaps, and particularly those between the Brillouin zone centre and the zone boundary, are systematically reduced for the off-stoichiometric sample. This effect is more pronounced at 930 °C than at 20 °C. In the case of $Fe_{80}Si_{20}$ certain gaps have completely collapsed at 1100 °C. Narrowing and disappearance of gaps are a consequence of successive

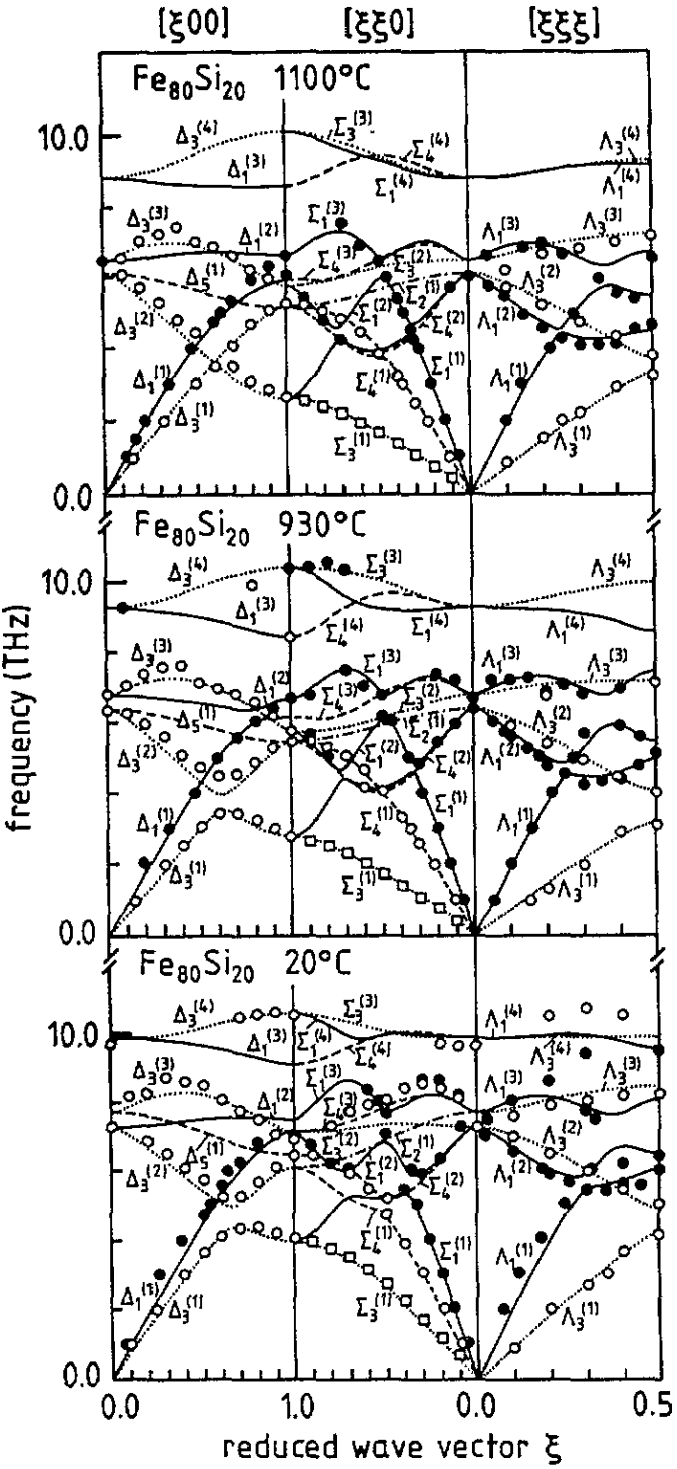

Figure 3. $Fe_{80}Si_{20}$: phonon dispersion at 20, 930 and 1100 °C. The lines correspond to a BVK fit assuming DO_3 structure and interactions between up to fourth nearest neighbours.

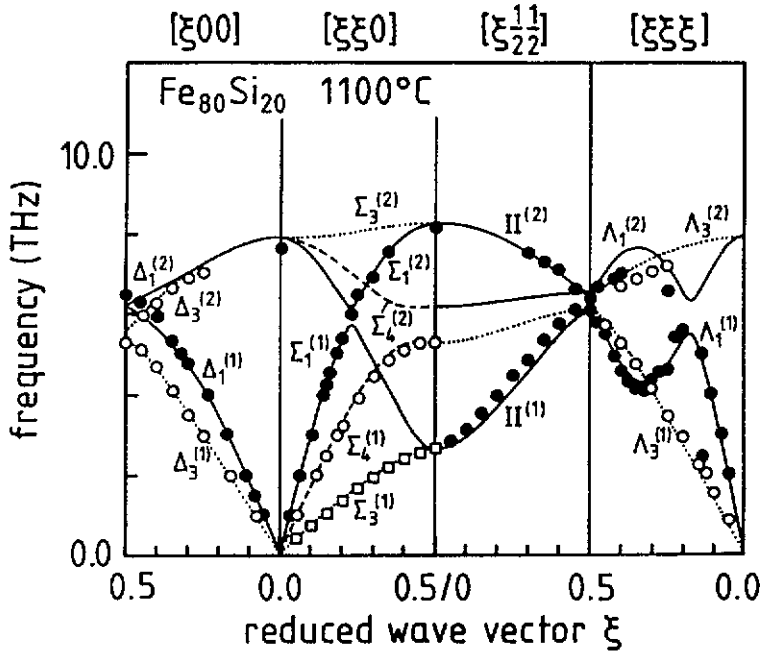

Figure 4. $Fe_{80}Si_{20}$: phonon dispersion at 1100 °C. The lines correspond to a BVK fit assuming B2 structure and interactions between up to fifth nearest neighbours.

disordering: the occupation of γ sites by antistructure atoms leads to a narrowing of the mass gaps even at room temperature. According to the continuous character of the order–disorder phase transition, this effect is more pronounced at elevated temperatures close to the transition. Once the off-stoichiometric sample is heated to 1100 °C, i.e. above the nominal transition temperature (in other words, the temperature at which the rate of decrease of the degree of order with increasing temperature has a maximum) to the B2 structure (1075 °C), certain gaps disappear. An interpretation of the measured phonon frequencies in the reduced scheme of B2 instead of that of $D0_3$ (compare the top part of figure 3 to figure 4) reduces drastically the number of independent phonon branches, e.g. to a maximum of six in [$\xi\xi$0] direction. This disappearance of phonon gaps is shown by way of example in figure 5 for the phonon gap between the transverse branches $\Delta_3^{(1)}$ and $\Delta_3^{(2)}$ of the $D0_3$ structure at $\xi = 0.5$. Note that the peak at 1100 °C is roughly twice as broad as the individual peaks at lower temperatures. A similar broadening is found for the whole $\Pi^{(1)}$ branch.

Thirdly, the phonon peaks of the highest optical branches, which are well characterized and clearly separated at room temperature, degenerate to a broad and structureless inelastic intensity distribution at 1100 °C. These intensities are found all over reciprocal space and extend from roughly 8 THz to a maximum of 11 THz. Consequently, no discrete phonon frequencies can be identified in the region of the highest optical band. For example, figure 6 shows the temperature dependence of the Brillouin zone boundary excitation at $Q = (0, 3, 3)$.

In this context it is useful to consider the influence of the different disordering models presented above on the phonon dispersion. A transition to ideal B2 implies (i) a complete collapse of certain phonon gaps and (ii) the disappearance of the highest optical band. Because the composition of our samples is far from that for ideal B2 ($Fe_{50}Si_{50}$), β and γ

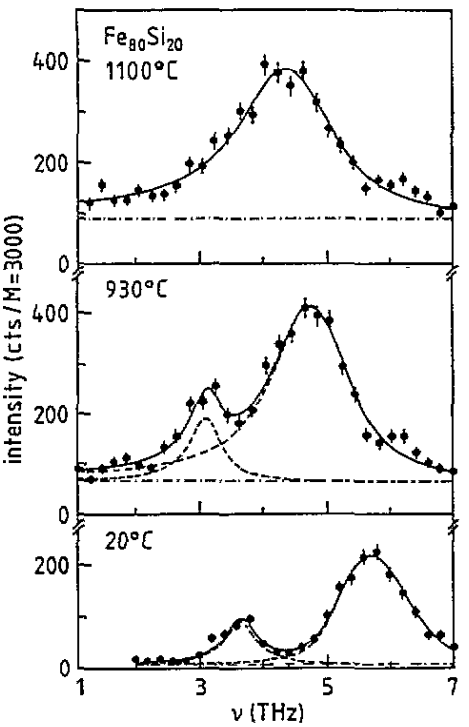

Figure 5. $Fe_{80}Si_{20}$: temperature dependence of the phonon gap between the transverse branches $\Delta_3^{(1)}$ and $\Delta_3^{(2)}$ at $\xi = 0.5$ ($Q = (1.5, 3, 3)$). The gap, clearly visible at room temperature, becomes narrower at 930 °C and disappears completely at 1100 °C. (Note that the corresponding phonon in the B2 structure is to be found in the $\Pi^{(1)}$ branch at $\xi = 0.5$.)

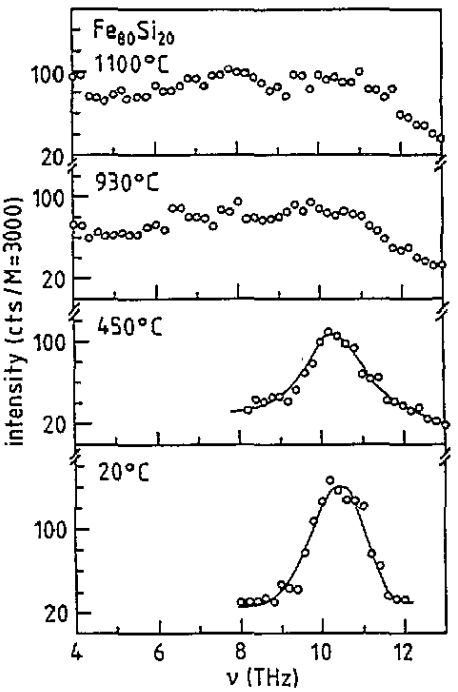

Figure 6. $Fe_{80}Si_{20}$: evolution as a function of temperature of the highest optical excitations at the Brillouin zone boundary $Q = (0, 3, 3)$. A well pronounced phonon group at room temperature degenerates to a broad inelastic intensity distribution at elevated temperatures. Lines are guides to the eye.

sites are, in first approximation, occupied randomly by Fe and Si atoms. We therefore further expect (iii) a broadening in energy of whole phonon branches due to the fact that atoms of different masses occupy the same sites and fluctuations in the force constants occur at these sites. We call this phenomenon phonon disorder scattering due to fluctuations of mass and force constants. This argument implies (iv) that excitations in the highest optical band (formally not existing any longer) persist beyond the phase transition but are considerably broadened in energy. The phonons measured in the present work are consistent with all these expectations (i) through (iv).

If, alternatively, the high-temperature phase is composed of relatively small DO_3-ordered domains, separated by antiphase boundaries, as found by Hilfrich *et al* (1994) (they give a domain size of 13 lattice parameters for $Fe_{80}Si_{20}$ at 1100 °C), scattering of phonons at the antiphase boundaries has to occur. In that case the highest optical band should not disappear, but—similar to the case mentioned above—a broadening of whole phonon branches is expected. However, because the DO_3 structure is maintained, phonon gaps at relatively short wavelengths should not disappear completely. One would rather expect that phonon gaps such as those shown in figure 5 will be filled by additional antiphase boundary scattering. The fact that figure 5 shows a collapse of the two phonons rather than a broad inelastic distribution of scattering events and a general lowering of phonon frequencies at

large q indicate that for our purposes a description of the high-temperature disorder in terms of a B2 structure and additional phonon disorder scattering may be more appropriate. Therefore, in figure 4 the phonon dispersion of $Fe_{80}Si_{20}$ at 1100 °C is also presented, as fitted with an underlying B2 structure. Further support for this interpretation comes from diffraction measurements (see next section).

4.2. Born–von Kármán (BVK) fits

As mentioned above, we use a BVK model with longitudinal and transverse springs (L–T model), which means that there are two force constants per atom pair and nearest neighbour. It can be shown that up to the second nearest neighbour this is equivalent to a tensor force model; from the third nearest neighbour, a tensor model involves more force constants. As the interactions in all the DO_3 alloys studied (Van Dijk 1970a, b, Zolliker 1992) were found to be short-ranged, the limitation to an L–T model seems reasonable. This is corroborated by the findings of Robertson (1991), who fitted Van Dijk's data with a sixth-nearest-neighbour tensor force model (35 fitting parameters!). The force constants he gives for the first three shells deviate only slightly from those given by Van Dijk (11-parameter BVK fit).

The number of shells that have to be taken into account is found by trial: the set of fitting parameters is increased until the fit quality does not improve any more. We found that in the case of DO_3 order a set of 16 force constants (corresponding to interactions between up to fourth nearest neighbours) was sufficient. In the B2 case the number of force constants is reduced by the higher symmetry—we used 14 fitting parameters (interactions between up to fifth nearest neighbours).

Of course, the order of the alloy has to be taken into account when the BVK fit is performed. To this aim we performed neutron diffraction measurements on powder samples of the same concentration and at the same temperatures as in the phonon measurements. Details of these measurements carried out on the DMC spectrometer at the PSI (Switzerland) are reported elsewhere (Randl *et al* 1994). The results relevant for the present work are summed up in table 1.

Table 1. Occupation probabilities O of the different sites for the alloys and temperatures examined, as obtained from a Rietveld fit to neutron powder diffraction patterns (Randl *et al* 1994).

Alloy	T (°C)	$O(\alpha)$	$O(\beta)$	$O(\gamma)$
$Fe_{75}Si_{25}$	20	Fe: 1.00	Fe: 0.00	Fe: 1.00
		Si: 0.00	Si: 1.00	Si: 0.00
	930	Fe: 1.00	Fe: 0.00	Fe: 1.00
		Si: 0.00	Si: 1.00	Si: 0.00
$Fe_{80}Si_{20}$	20	Fe: 1.00	Fe: 0.20(8)	Fe: 1.00
		Si: 0.00	Si: 0.80(8)	Si: 0.00
	930	Fe: 1.00	Fe: 0.28(2)	Fe: 0.92(2)
		Si: 0.00	Si: 0.72(2)	Si: 0.08(2)
	1100	Fe: 1.00	Fe: 0.63(9)	Fe: 0.57(9)
		Si: 0.00	Si: 0.37(9)	Si: 0.43(9)

Within the accuracy of the Rietveld fit (Rietveld 1969), estimated to be of the order of 3 at.%, we do not find an indication for disorder in $Fe_{75}Si_{25}$, even at 930 °C. In $Fe_{80}Si_{20}$, however, there has to be disorder: the relative excess of Fe atoms is made up by creation of Fe antistructure defects in the β sublattice. At 930 °C we observe additional disorder:

about 8% of the γ sites are occupied by Si atoms, whereas the percentage of the Fe atoms in the β sublattice has increased by the same amount. Finally, at 1100 °C the diffraction pattern can be fitted by an almost perfect B2 structure (see preceding section).

This structural information was taken into account for the BVK fits by attributing averaged masses to the different sites.

One crucial difficulty concerning the BVK fits consists of the correct attribution of measured phonons to the theoretically expected phonon branches; errors in the attribution may lead to completely misleading results. Reliability is obtained by an iterative process. After first (and easily identifiable) phonon groups have been measured, a preliminary BVK fit is carried out, and the phonon structure factors for the different branches are determined. Knowledge of the structure factors allows one to find the region in reciprocal space where the phonon can be identified most easily and measured with highest intensity. Thus, the dispersion is completed, which allows one to calculate improved phonon structure factors, and so on. The structure factors for Fe_3Si of $D0_3$ and B2 structure can be found in Randl (1994).

Table 2 lists the force constants obtained for $Fe_{75}Si_{25}$ and $Fe_{80}Si_{20}$ at 20 and 930 °C, as well as the values given by Van Dijk (1970a, b) for $Fe_{75}Al_{25}$ at 20 °C. The force constants of B2-ordered $Fe_{80}Si_{20}$ at 1100 °C are given in table 3.

Table 2. Interatomic force constants (N m^{-1}) of $Fe_{75}Al_{25}$ (after Van Dijk 1970a, b), $Fe_{75}Si_{25}$ and $Fe_{80}Si_{20}$ ($D0_3$ fit).

	$Fe_{75}Al_{25}$	$Fe_{75}Si_{25}$		$Fe_{80}Si_{20}$		
	20 °C	20 °C	930 °C	20 °C	930 °C	1100 °C
$L_1(12)$	43.5(9)	55.7(2)	47.0(6)	52.7(2)	39.2(9)	34.4(5)
$T_1(12)$	0.4(5)	−2.7(2)	−3.7(3)	−3.2(2)	−1.8(2)	−1.6(3)
$L_1(23)$	56.5(7)	42.1(2)	44.1(2)	51.8(2)	56.3(5)	61.1(1.6)
$T_1(23)$	−1.7(4)	0.7(2)	−2.2(2)	0.3(2)	−2.9(3)	−6.4(3)
$L_2(13)$	11.1(7)	8.0(2)	11.1(4)	12.0(3)	14.8(4)	15.6(5)
$T_2(13)$	−2.4(4)	2.0(3)	−3.1(4)	1.8(3)	0.1(3)	0.8(4)
$L_2(24)$	3.1(5)	15.9(4)	17.3(8)	18.0(3)	11.3(2)	12.4(3)
$T_2(24)$	0.8(3)	1.8(3)	−0.7(4)	2.7(2)	−1.8(5)	−1.8(4)
$L_3(11)$	4.0(4)	8.6(3)	8.8(6)	6.5(3)	8.5(3)	3.2(3)
$T_3(11)$	—	−0.1(2)	−2.5(2)	0.0(2)	−3.9(4)	−1.5(3)
$L_3(22)$	3.0(2)	2.0(2)	−1.6(5)	1.3(2)	0.7(3)	1.4(3)
$T_3(22)$	—	−0.3(2)	1.8(3)	−0.3(2)	0.8(3)	−0.1(2)
$L_3(33)$	0.6(4)	4.5(3)	3.3(6)	2.1(3)	−3.9(5)	2.8(6)
$T_3(33)$	—	−0.4(2)	−1.8(2)	−1.1(2)	−0.6(3)	1.8(3)
$L_4(12)$	—	−1.8(2)	−1.2(2)	−1.7(2)	−0.2(2)	−2.7(3)
$L_4(23)$	—	0.6(2)	0.9(2)	0.3(2)	−0.1(2)	1.8(2)

When trying to interpret the force constants, one should keep in mind that a BVK fit is above all a useful way of parametrizing dispersion relations without deep physical significance. Nevertheless, some conclusions may be drawn. In Fe_3Al, as in Fe_3Si, the nearest-neighbour Fe–Fe and Fe–(Al,Si) interactions are dominant and of the same order of magnitude ($L_1(12) \simeq L_1(23) \gg L_2(13), L_2(24), \ldots$). In Fe_3Al the Fe–Al interaction is a little stronger than its Fe–Fe counterpart ($L_1(23) > L_1(12)$), which is also found in $Fe_{80}Si_{20}$ (especially at high temperatures), whereas the contrary appears to be true

Table 3. Interatomic force constants (N m^{-1}) of $Fe_{80}Si_{20}$ at 1100° (B2 fit).

$L_1(12)$	38.2(3)
$T_1(12)$	−1.2(3)
$L_2(11)$	2.8(3)
$T_2(11)$	1.3(3)
$L_2(22)$	9.0(4)
$T_2(22)$	−0.5(4)
$L_3(11)$	2.1(4)
$T_3(11)$	−2.2(4)
$L_3(22)$	−1.0(4)
$T_3(22)$	1.4(3)
$L_4(12)$	1.1(3)
$T_4(12)$	−0.4(3)
$L_5(12)$	0.5(3)
$T_5(12)$	0.0(3)

in stoichiometric Fe_3Si. This correlates to the experimental finding that the gaps in the dispersion of Fe_3Al (see Van Dijk 1970a, b) are much narrower than in $Fe_{75}Si_{25}$, similar to the $Fe_{80}Si_{20}$ alloy at high temperatures. It is also remarkable that the interactions between more distant neighbours are, in general, stronger in the Fe_3Si alloys than in Fe_3Al.

The general 'softening' of the dispersion with increasing temperature is reflected in a general decrease of the force constants. It is, of course, difficult to separate the effects of temperature (lattice expansion, anharmonicities, ...) and disorder. The effect is pronounced for Fe–Fe pairs (12) whereas the force constants increase for Fe–Si pairs (23, 13).

The dependence of the force constants on the alloy composition is more complex and difficult to interpret, all the more so as many parameters are changed (site occupancies, average masses, lattice parameters, ...). There is some evidence that the NN Fe–Fe interaction becomes weaker with growing Fe content, whereas the interaction between the atoms on the α and β sites is strengthened by the additional Fe atoms on the latter sites.

4.3. Phonon widths

We did not find significant changes of phonon widths as a function of alloy concentration. There is, however, a distinct temperature effect. This will be demonstrated in the case of the $\Sigma_3^{(1)}$ or $T_1[\xi\xi 0]$ branch (polarization $[\xi\ -\xi 0]$). Figure 7 shows the dependence of the widths observed on the reduced wavevector ξ and temperature for both alloys. It is found that there is no distinct broadening at room temperature in both alloys, but at high temperatures the phonons clearly broaden with increasing wavevector. Most probably this is related to increasing disorder. The order–disorder transitions in Fe_3Si are of second or higher order and diffusion-driven, so we do not expect strong phonon softening and broadening concentrated around one particular wavevector, as found, for instance, for the displacive transitions in the high-temperature BCC phases of several metals (see, for example, Petry *et al* 1991a, b). The continuous increase in phonon width rather reflects the continuous increase of disorder with increasing temperature.

4.4. Elastic constants

The elastic constants of the alloys we have examined can be determined from the initial slope of the dispersion relation and compared to the values obtained by ultrasound velocity

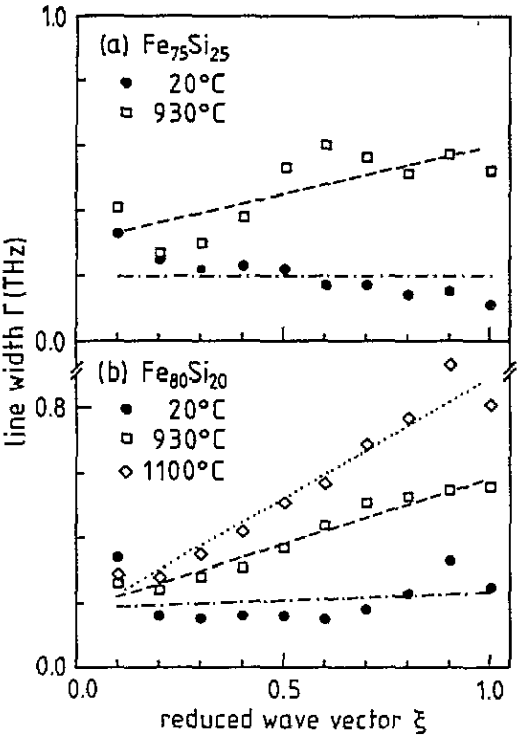

Figure 7. Wavevector dependence of the phonon width Γ (damped oscillator, resolution deconvoluted) of the $T_1[\xi\xi 0]$ or $\Sigma_3^{(1)}$ branch (polarization $[\xi - \xi 0]$) for the different alloy compositions and temperatures.

measurements. In general, the latter values are more precise because it is difficult for inelastic neutron scattering to separate the acoustic phonons at very small wavevector from the elastic intensity. Therefore, one often imposes the elastic constants as boundary conditions to the BVK fits.

Unfortunately, for both alloys, $Fe_{75}Si_{25}$ and $Fe_{80}Si_{20}$, values of the elastic constants are only available for room temperature and below (Kötter *et al* 1989 and references therein). We have imposed these literature values to the BVK fits for the dispersion relations measured at room temperature (thereby reducing the number of free parameters by three), whereas all other dispersions have been fitted without such a constraint. As can be seen from figures 2 and 3, the initial slopes of the BVK fit for the room-temperature dispersions fit only moderately to the initial slopes as measured by neutrons, which is due to the additional constraints. This phenomenon is known as the difference between first and zero sound, due to the interaction of the elastic waves with other excitations. The lifetimes of excitations in anharmonic crystals are about 10^{-11} s. As the frequencies used in the ultrasound velocity measurements are of the order of 10^7 Hz, the mode of propagation is influenced by collisions with these excitations (first sound). The phonon frequencies, however, are of the order of 10^{12} Hz, which does not allow thermodynamic equilibrium to be established: the wave propagates in a collision-free mode (zero sound). Thus, the difference between the initial slopes in the phonon dispersion (phonon data) and those expected from ultrasonic measurements (BVK fit) gives an impression of the degree of anharmonicity of the lattice vibrations. Table 4 gives all the elastic constants as calculated

Table 4. The elastic constants of $Fe_{75+x}Si_{25-x}$ (units: 10^{10} N m^{-2}). The room-temperature values have been taken from Kötter *et al* (1989) and kept fixed in the BVK fits. The other data sets have been calculated from the BVK force constants.

Alloy	T (°C)	a (Å)	C_{11}	C_{44}	C_{12}	$C' = (C_{11} - C_{12})/2$
$Fe_{75}Si_{25}$	20	5.64	21.9	13.7	14.3	3.8
	930	5.74	21.3	8.8	16.6	2.4
$Fe_{80}Si_{20}$	20	5.67	21.6	13.3	14.6	3.5
	930	5.76	19.8	9.1	15.9	1.9
	1100	5.78	19.7	9.4	16.0	1.9

from the BVK force constants.

4.5. Density of states

The normalized density of states $Z(\nu)$ can be obtained from the dispersion relation $\nu_s(q)$ by an integration over the Brillouin zone:

$$Z(\nu)\,\mathrm{d}\nu = \sum_s \int_{\nu<\nu_s<\nu+\mathrm{d}\nu} \left|\frac{\mathrm{d}\nu_s(q)}{\mathrm{d}q}\right|^{-1} \mathrm{d}q \left(3N_C \int \mathrm{d}q\right)^{-1}.$$

The sum runs over the s phonon branches. N_C is the number of atoms in the elementary unit cell. The integration is most commonly carried out numerically by scanning the Brillouin zone in a way first proposed by Gilat and Raubenheimer (1966).

The calculated densities of states for the two alloys at the various temperatures are shown in figure 8. Of course, these densities reflect the dispersion curves. Contrary to the case of Fe_3Al, where only small mass gaps are found (see Van Dijk 1970a, b), $Fe_{75}Si_{25}$ shows distinct gaps at room temperature, which results in a separation of $Z(\nu)$ into four different parts. At 930 °C, two gaps are still visible, but all the frequencies have shifted to lower values. In $Fe_{80}Si_{20}$ all gaps below the highest optical band are less pronounced, tend to vanish at 930 °C and are no longer visible at 1100 °C. The highest optical band and the corresponding gap at 1100 °C are a pure artefact of the DO_3 fit to a phonon dispersion of a crystal that has adopted the B2 structure. However, we again emphasize that the neutron spectra clearly indicate the presence of a broad density of states extending without a gap from 8 THz to a maximum of 11 THz (figure 6). As discussed in a preceding section we attribute this to a band of disorder scattering caused by both mass and force constant fluctuations.

4.6. Mean square displacement and Debye temperature

In the case of a cubic Bravais crystal one can easily calculate thermodynamic quantities from the density of states. The mean square displacement $\langle u_\alpha^2 \rangle$ of the atoms in a direction α is given as

$$\langle u_\alpha^2 \rangle = \frac{h}{8\pi^2 M} \int_0^\infty \frac{1}{\nu} \coth\left(\frac{h\nu}{2k_B T}\right) Z(\nu)\,\mathrm{d}\nu$$

where h is the Planck constant, M is the atomic mass, k_B is the Boltzmann constant and T is the absolute temperature. Owing to the weighting by $1/\nu$, $\langle u_\alpha^2 \rangle$ is essentially determined by the low-energy phonons.

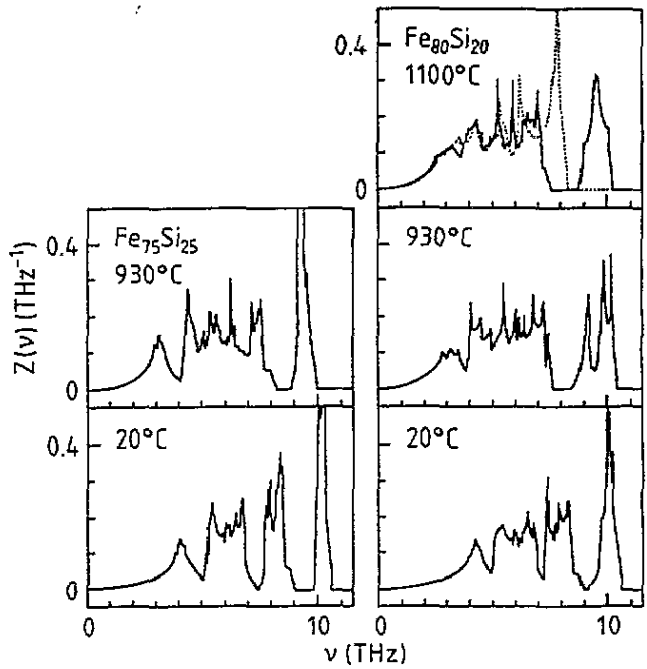

Figure 8. Phonon density of states for the different alloys and temperatures studied, as calculated from the BVK force constants ($D0_3$ fit). For $Fe_{80}Si_{20}$ at 1100 °C the density of states corresponding to the B2 fit is also given (dotted line).

The Debye temperature Θ_D can be obtained from $\langle u_\alpha^2 \rangle$ through:

$$\langle u_\alpha^2 \rangle = \frac{3h^2}{4\pi^2 k_B \Theta_D M}\left(\frac{1}{4} + \frac{T^2}{\Theta_D^2}\int_0^{\Theta_D/T} dx \frac{x}{e^x - 1}\right).$$

The values found here are in good agreement with other evaluations of $\langle u_\alpha^2 \rangle$ and Θ_D. For the $Fe_{80}Si_{20}$ alloy at 1100 °C the thermodynamic quantities have been calculated for both the $D0_3$ and the B2 structures. Because $\langle u_\alpha^2 \rangle$ and Θ_D are dominated by low-energy and large-amplitude phonons, their values are identical for both structures within error bars. For the sake of consistency table 5 contains only the values for the $D0_3$ fits.

Table 5. Thermodynamic quantities derived from the phonon densities of states; $\langle u_\alpha^2 \rangle^*$, determined from diffraction measurements, is given for the sake of comparison.

Alloy	T (°C)	H_m (eV)	$\langle u_\alpha^2 \rangle$ (10^{-2} Å^2)	$\langle u_\alpha^2 \rangle^*$ (10^{-2} Å^2)	Θ_D (K)
$Fe_{75}Si_{25}$	20	0.59(2)	0.47(2)	0.3(2)	444 ± 7
	930	0.41(2)	2.7(1)	3.1(1)	364 ± 7
$Fe_{80}Si_{20}$	20	0.60(2)	0.46(2)	0.5(1)	437 ± 7
	930	0.40(2)	2.8(1)	2.4(1)	354 ± 7
	1100	0.39(2)	3.3(1)	3.4(1)	348 ± 7

The Rietveld analysis of our diffraction data was performed with the isotropic mean square displacement as a free parameter. The values for $\langle u_\alpha^2 \rangle$ obtained from both phonon

densities and Bragg intensities are compared in table 5. The agreement is fair; the values from the phonon measurements are expected to be more precise. Sepiol (1994) has determined the Debye temperature of the Fe atoms in $Fe_{75}Si_{25}$ from Mössbauer intensities between 20 and 500 °C and finds a value of 369 ± 3 K.

4.7. Migration enthalpy

Finally, the migration enthalpy H_m has been derived. Schober *et al* (1992) give the following expression

$$H_m = 4\pi^2 a^2 \alpha \left(\int \frac{Z(\nu)}{M\nu^2} \, d\nu \right)^{-1}$$

where a is the lattice parameter, α is a constant (0.0130(7) for BCC structures) and M is the atomic mass. The corresponding figures of H_m are also listed in table 5. By the same reasoning as in the preceding section the value of H_m for the $Fe_{80}Si_{20}$ alloy at 1100 °C does not differ significantly when either the DO_3 or the B2 structure is chosen. Strictly speaking, this formula for H_m is only valid for monatomic structures. The underlying *ansatz* assumes diffusion to take place via nearest-neighbour jumps in {111} directions, which is the case in Fe_3Si (see Sepiol and Vogl 1993). Therefore, as a first approximation, we consider the DO_3 structure as a BCC lattice of half the lattice parameter of the DO_3 cell and atoms of a mass corresponding to the average mass of the four atoms of the DO_3 cell. Such a calculation can only be a first guess: we do not make any difference between Fe and Si atoms, nor do we take into consideration microscopic details of the jump mechanism, for instance that in Fe_3Si the Fe atoms do not jump to Si sites. However, the *ansatz* takes into account information from the low-energy phonons: they indicate in which directions the interatomic potentials have low restoring forces, i.e. where the atoms are allowed to vibrate with larger amplitudes. Our model for H_m assumes that the diffusion jump—the most anharmonic event one can think of—follows a trajectory similar to the direction of low—harmonic—restoring forces. In other words: in the directions where the harmonic part of the potential is low, we expect the anharmonic part, i.e. the migration barrier, to be of low energy as well.

In fact, there are some findings in favour of this microscopic picture. First, the transverse phonons with $[\xi\xi 0]$ propagation and $[\xi\ -\xi 0]$ polarization are of lowest energy, as in the BCC metals (Petry *et al* 1991a, b). The corresponding phonon displacements push atoms in the direction of nearest-neighbour sites. Secondly, this very phonon branch reflects great anharmonicities of the corresponding interatomic potential; the phonon frequencies decrease most strongly with temperature and the phonon lifetime reduces drastically with temperature (figure 7).

The values of H_m at high temperatures (listed in table 5) are roughly 1.3 to 1.5 times higher than those found for β-Ti or β-Zr. The comparison to these metals is justified by the fact that the diffusivities are of similar order of magnitude (Vogl and Sepiol 1994). H_m decreases with increasing temperature, and—within error bars—there is no difference between the two concentrations. This is also visible in the phonon dispersions: the $\Sigma_3^{(1)}$ branch of the Fe_3Si alloys is of higher energy than the corresponding branches in the mentioned BCC metals, and $\Sigma_3^{(1)}$ is almost independent of the alloy composition.

The relatively low migration barriers are in accordance with the high diffusivities of Fe in the stoichiometric alloy, but their composition dependence is in strong disagreement with the diffusion data. As Sepiol and Vogl (1993) have shown, the Fe diffusivity in $Fe_{75}Si_{25}$ is about 10 times higher than in $Fe_{80}Si_{20}$, and this strong concentration dependence has been confirmed by recent tracer measurements (Gude *et al* 1994). As the phonon dispersions do not reflect at all such a drastic change, one has to conclude that the migration barrier alone *cannot* account for fast diffusion.

4.8. Vacancy concentration

It has been proposed that diffusion in intermetallic alloys might be enhanced by an unusually high concentration of structural vacancies (see, for example, Wever *et al* 1989). In the case of Ni_3Sb, Heumann and Stüer (1966) have argued that structural vacancies of the order of up to 10% were present, and this has been confirmed directly by neutron diffraction (Randl *et al* 1994). Similar vacancy concentrations are suspected to be present in Fe_3Al (Kentzinger *et al* 1995), and positron annihilation experiments performed by Schaefer *et al* (1990) indicated high vacancy densities at high temperatures.

Is there evidence for high vacancy concentrations in Fe_3Si as well? If the vacancy concentration in Fe_3Si is of the order of several per cent *and* if these vacancies show a preference for one sublattice, for instance, the α sites (as is the case in Ni_3Sb), one would find a measurable alteration of the Bragg intensities. As mentioned above, powder diffraction measurements have been performed to that purpose (Randl *et al* 1994). The Rietveld analysis of the diffraction patterns shows that the off-stoichiometric samples are disordered, as was to be expected (see table 1). However, no indications of unusual vacancy concentrations in one preferential sublattice have been found. However, this does not mean that there are not an extraordinarily high concentration of vacancies: if they are present, they simply have to be distributed isotropically and contribute to the diffuse background only.

5. Conclusions

Phonon dispersions in $Fe_{75}Si_{25}$ and $Fe_{80}Si_{20}$ have been measured at temperatures between 20 and 1100 °C. In agreement with the phase diagram, the dispersion of the stoichiometric alloy clearly reflects the highly ordered DO_3 structure. For this sample there is evidence for disordering up to 930 °C. The phonons in the off-stoichiometric sample, however, clearly indicate that disorder increases with increasing temperature: DO_3 phonon gaps visible at room temperature diminish (at 930 °C) and disappear completely (at 1100 °C) as the temperature is raised. Well structured and clearly separated peaks of the highest optical branches present at low temperatures degenerate into a broad and dispersionless band of excitations at 1100 °C. There is no gap separating this band from the excitations at lower energies. The dispersion of the off-stoichiometric sample at 1100 °C can be well fitted in terms of the less-ordered B2 structure. The presence of this additional intensity is then interpreted in terms of phonon disorder scattering.

Transverse acoustic phonon branches are of low energy, which indicates low potential barriers for nearest-neighbour diffusion jumps. However, the migration enthalpies that we calculate do not vary as a function of the alloy composition, i.e. they cannot be responsible for the pronounced decrease of the Fe diffusivity found in off-stoichiometric alloys.

Alternatively, we propose that diffusion in $Fe_{1-x}Si_x$ (with x around 25%) is controlled by a high concentration of vacancies. Diffraction measurements designed to check this hypothesis did not give direct evidence for a high vacancy density, but they do not exclude a high concentration of vacancies distributed homogeneously among the different sublattices.

Further measurements using the Simmons–Baluffi method or positron annihilation are proposed in order to measure the vacancy concentration directly.

Acknowledgments

We wish to thank W Bührer and F Altorfer for making it possible to perform accompanying diffraction measurements at the PSI (Switzerland). One of the authors (OGR) is indebted to L Pintschovius for help and discussions during one of the beam-times in Saclay. Financial support by the Austrian Fonds zur Förderung der Wissenschaftlichen Forschung (FWF), Contracts S5601 and S5605, is gratefully acknowledged.

References

Dokken R N 1965 *Trans. AIME* **233** 1187
Feldwisch R, Sepiol B and Vogl G 1995 *Acta Metall. Mater.* **43** 2033
Gilat G and Raubenheimer L J 1966 *Phys. Rev.* **144** 390
Gude A, Mehrer H and Sepiol B 1994 *Verhandl. DPG* (VI) **29** 307
Heumann T and Stüer H 1966 *Phys. Status Solidi* **15** 95
Hilfrich K, Kölker W, Petry W, Schärpf O and Nembach E 1993 *Z. Metallkd.* **84** 255
—— 1994 *Acta Metall. Mater.* **42** 743
Ibel K (ed) 1994 *Guide to Neutron Research Facilities at the ILL* (Grenoble: ILL)
Kentzinger E, Cadeville M C, Pierron-Bohnes V, Petry W and Hennion B 1995 to be published
Kötter G, Nembach K, Wallow F and Nembach E 1989 *Mater. Sci. Eng.* A **114** 29
Kubaschewski O 1982 *Iron–Binary Phase Diagrams* (Berlin: Springer)
Mori M, Yamada Y and Shirane G 1975 *Solid State Commun.* **17** 127
Morii Y and Iizumi M 1985 *J. Phys. Soc. Japan* **54** 2848
Petry W, Heiming A, Herzig C and Trampenau J 1991a *Defect Diffus. Forum* **75** 211
Petry W, Heiming A, Trampenau J, Alba M, Herzig C, Schober H R and Vogl G 1991b *Phys. Rev.* B **43** 10 933
Petry W, Heiming A, Trampenau J and Vogl G 1989 *Defect Diffus. Forum* **66–69** 157
Pintschovius L 1987 *Phys. Rev.* B **35** 5175
Randl O G 1994 *Thesis* Institut für Festkörperphysik, University of Vienna
Randl O G, Vogl G, Sepiol B, Bührer W and Altorfer F 1994 *Annual LNS Progress Report* ETH Zürich and PSI, to be published
Rausch J B and Kayser F X 1977 *J. Appl. Phys.* **48** 487
Rietveld H M 1969 *J. Appl. Crystallogr.* **2** 65
Rixecker G, Schaaf P and Gonser U 1993 *Phys. Status Solidi* a **139** 309
Robertson I M 1985 *Solid State Commun.* **53** 901
—— 1991 *J. Phys.: Condens. Matter* **3** 8181
Schaefer H E, Würschum R, Sob M, Zak T, Yu W Z, Eckert W and Banhart F 1990 *Phys. Rev.* B **41** 11 869
Schober H R, Petry W and Trampenau J 1992 *J. Phys.: Condens. Matter* **4** 9321
Sepiol B 1994 private communication
Sepiol B and Vogl G 1993 *Phys. Rev. Lett.* **71** 731
Sepiol B, Randl O G, Karner C, Heiming A and Vogl G 1994 *J. Phys.: Condens. Matter* **6** L43
Van Dijk C 1970a *Thesis* Reactor Centrum Nederland, Petten, RCN-129
—— 1970b *Phys. Lett.* **32A** 255
Vogl G, Randl O G, Petry W and Hünecke J 1993 *J. Phys.: Condens. Matter* **5** 7215
Vogl G and Sepiol B 1994 *Acta Metall. Mater.* **42** 3175
Wever H, Hünecke J and Frohberg G 1989 *Z. Metallkd.* **80** 389
Zolliker M 1992 *Thesis* ETH Zürich, No 9577